A Non-Parametric Test to Detect Data-Copying in Generative Models

Casey Meehan Kamalika Chaudhuri Sanjoy Dasgupta
University of California, San Diego

Abstract

Detecting overfitting in generative models is an important challenge in machine learning. In this work, we formalize a form of overfitting that we call *data-copying* – where the generative model memorizes and outputs training samples or small variations thereof. We provide a three sample test for detecting data-copying that uses the training set, a separate sample from the target distribution, and a generated sample from the model, and study the performance of our test on several canonical models and datasets.

1 Introduction

Overfitting is a basic stumbling block of any learning process. While it has been studied in great detail in the context of supervised learning, it has received much less attention in the unsupervised setting, despite being just as much of a problem.

To start with a simple example, consider a classical kernel density estimator (KDE), which given data $x_1, \ldots, x_n \in \mathbb{R}^d$, constructs a distribution over $\mathbb{R}^d$ by placing a Gaussian of width $\sigma > 0$ at each of these points, yielding the density

$$q(x) = \frac{1}{(2\pi)^{d/2}\sigma^d n} \sum_{i=1}^{n} \exp\left(-\frac{\|x - x_i\|^2}{2\sigma^2}\right). \qquad (1)$$

The only parameter is the scalar σ. Setting it too small makes $q(x)$ too concentrated around the given points: a clear case of overfitting (see Appendix **Figure 6**). This cannot be avoided by choosing the σ that maximizes the log likelihood on the training data, since in the limit $\sigma \to 0$, this likelihood goes to ∞. One solution here is to instead maximize log-likelihood on a held-out validation set.

Proceedings of the 23[rd]International Conference on Artificial Intelligence and Statistics (AISTATS) 2020, Palermo, Italy. PMLR: Volume 108.

If even the one-parameter kernel density estimator is capable of overfitting, the situation is truly treacherous for the enormously complex generative models that have emerged over the past decade or so. Variational Auto Encoders (VAEs) (Kingma and Welling, 2013) and Generative Adversarial Networks (GANs) (Goodfellow et al., 2014) for example can easily involve millions of parameters. A major challenge in evaluating overfitting in these models is that most do not offer exact, tractable likelihoods. VAEs can only tractably provide a likelihood lower bound, while GANs have no accompanying density estimate at all. Thus any method that can assess these generative models must be based only on samples produced by them.

A body of prior work has provided tests for evaluating generative models based on samples drawn from them (Salimans et al., 2016; Sajjadi et al., 2018; Wu et al., 2017; Heusel et al., 2017); however, the vast majority of these tests focus on 'mode dropping' and 'mode collapse': the tendency for a generative model to either merge or delete high-density modes of the true distribution. A generative model that simply reproduces the training set or minor variations thereof will pass most of these tests.

In contrast, in this work we formalize and investigate a particular type of overfitting that we call 'data-copying': the propensity of a generative model to recreate minute variations of a subset of training examples it has seen, rather than represent the true diversity of the data distribution. An example is shown in **Figure 1b**; in the top region of the instance space, the generative model data-copies, or creates samples that are very close to the training samples; meanwhile, in the bottom region, it underfits. To detect this, we introduce a data-copying hypothesis test that relies on three independent samples: the original training sample used to produce the generative model; a separate (held-out) test sample from the underlying distribution; and a synthetic sample drawn from the generator.

Our key insight is that an overfit generative model would produce samples that are too close to the training samples – closer on average than an independently drawn test sample from the same distribution. Thus,

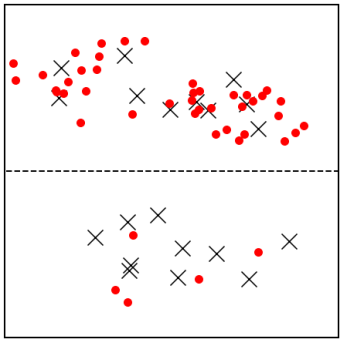

(a) Illustration of over-/under-representation
Training sample: ×, Generated sample: •

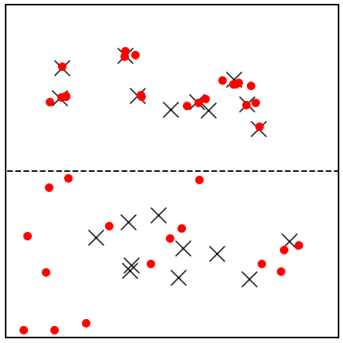

(b) Illustration of data-copying/underfitting
Training sample: ×, Generated sample: •

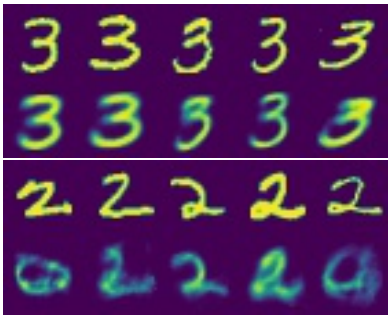

(c) VAE copying/underfitting on MNIST
top: $Z_U = -8.54$, bottom: $Z_U = +3.30$

Figure 1: Comparison of data-copying with over/under representation. Each image depicts a single instance space partitioned into two regions. Illustration **(a)** depicts an over-represented region (top) and under-represented region (bottom). This is the kind of overfitting evaluated by methods like FID score and Precision and Recall. Illustration **(b)** depicts a data-copied region (top) and underfit region (bottom). This is the type of overfitting focused on in this work. Figure **(c)** shows VAE-generated and training samples from a data-copied (top) and underfit (bottom) region of the MNIST instance space. In each 10-image strip, the bottom row provides random generated samples from the region and the top row shows their training nearest neighbors. Samples in the bottom region are on average further to their training nearest neighbor than held-out test samples in the region, and samples in the top region are closer, and thus 'copying' (computed in embedded space, see Experiments section).

if a suitable distance function is available, then we can test for data-copying by testing whether the distances to the closest point in the training sample are on average smaller for the generated sample than for the test sample. A further complication is that modern generative models tend to behave differently in different regions of space; a configuration as in **Figure 1b** for example could cause a global test to fail. To address this, we use ideas from the design of non-parametric methods by dividing the instance space into cells, conducting our test separately in each cell, and then combining the results to get a sense of the average degree of data-copying.

1.1 Related work

There has been a large body of prior work on the evaluation of generative models (Salimans et al., 2016; Lopez-Paz and Oquab, 2016; Richardson and Weiss, 2018; Sajjadi et al., 2018; Xu et al., 2018; Wu et al., 2017) . However, most are geared to detect some form of mode-collapse or mode-dropping: the tendency to either merge or delete high-density regions of the training data. Consequently, they fail to detect even the simplest case of extreme data-copying – where a generative model memorizes and exactly reproduces a bootstrap sample from the training set. We discuss below a few of these tests that use ideas similar to ours.

To-date there is a wealth of techniques for evaluating whether a model mode-drops or -collapses. Tests like the popular Inception Score (IS), Frechét Inception Distance (FID) (Heusel et al., 2017), Precision and Recall test (Sajjadi et al., 2018), and extensions thereof (Kynkäänniemi et al., 2019; Che et al., 2016) all work by embedding samples using the features of a discriminative network like 'InceptionV3' and somehow checking whether the training and generated distributions are similar *in aggregate*. The hypothesis-testing binning method proposed by Richardson and Weiss (2018) also compares aggregate population data, without embedding samples. The parametric Kernel MMD method proposed by Sutherland et al. (2016) uses a carefully selected kernel to estimate the distribution of both the generated and training samples and reports the maximum mean discrepancy between the two. Such tests will reward a generative model that only produces slight variations of the training set, since a 'good' aggregate distribution is defined by the training sample.

Lopez-Paz and Oquab (2016) propose the *Two-Sample Nearest Neighbor*, a two-sample non-parametric test. Their method groups a training and generated sample of equal cardinality together, with training points labeled '1' and generated points labeled '0', and then reports the Leave-One-Out (LOO) Nearest-Neighbor (NN) accuracy of predicting '1's and '0's. We report two values as discussed by Xu et al. (2018): the LOO accuracy of the training points, and the LOO accuracy of the generated points. An ideal generative model should produce an accuracy of 0.5 for each sample. Unlike this method, our test not only detects exact data-copying, which is unlikely, but estimates whether a given model generates samples closer to the training set than it should, as determined by a held-out test set.

The concept of data-copying has been explored by Xu et al. (2018) (where it is called 'memorization') for a variety of generative models and several of the above two-sample evaluation tests. Their results indicate that only the two-sample NN test is able to capture instances

of extreme data-copying. Similarly, Bounliphone et al. (2016) explores three-sample testing, but for comparing the performance of different models, not for detecting overfitting. Other works contemporary with this take parametric approaches to finding data copying via neural network divergences (Gulrajani et al., 2020) and via learning reverse mappings for latent code models (Webster et al., 2019). The present work departs from those by offering a probabilistically motivated non-parametric test that is entirely model agnostic.

2 A Hypothesis Test for Data Copying

Let $\mathcal{X}$ denote an instance space in which data points lie, and P an unknown underlying distribution on this space. A training set T is drawn from P and is used to select a generative model Q. We then wish to assess whether Q is the result of overfitting: that is, whether Q is too close to the training data. To help ascertain this, we are able to draw two additional samples: a fresh sample of n points from P called P_n; a sample of m points from Q; called this Q_m.

As illustrated in **Figures 1a, 1b**, generative model overfitting can occur locally in some subspace $\mathcal{C} \subseteq \mathcal{X}$. To characterize this for any distribution D on $\mathcal{X}$, let $D|_{\mathcal{C}}$ denote its restriction to the region $\mathcal{C}$, that is,

$$D|_{\mathcal{C}}(\mathcal{A}) = \frac{D(\mathcal{A} \cap \mathcal{C})}{D(\mathcal{C})} \quad \text{for any } \mathcal{A} \subseteq \mathcal{X}.$$

2.1 Types of Overfitting

We now formalize the distinction between data-copying and over-representation, starting with a probabilistic interpretation of data-copying.

Intuitively, overfitting refers to situations where Q is "too close" to the training set T; that is, closer to T than the target distribution P happens to be. To make this quantitative, we begin by choosing a distance function $d : \mathcal{X} \to \mathbb{R}$ from points in $\mathcal{X}$ to the training set, for instance, $d(x) = \min_{t \in T} \|x - t\|^2$, if $\mathcal{X}$ is a subset of Euclidean space.

Naturally, we desire that Q's expected distance to the training set is the same as that of P's, namely $\mathbb{E}_{X \sim P}[d(X)] = \mathbb{E}_{Y \sim Q}[d(Y)]$. We may rewrite this as follows: given any distribution D over $\mathcal{X}$, define $L(D)$ to be the one-dimensional distribution of $d(X)$ for $X \sim D$. We consider overfitting to have occurred if random draws from $L(P)$ are systematically larger than from $L(Q)$. The above equalized expected distance condition can be redrafted as

$$\mathbb{E}_{Y \sim Q}[d(Y)] - \mathbb{E}_{X \sim P}[d(X)] = \mathbb{E}_{\substack{A \sim L(P) \\ B \sim L(Q)}}[B - A] = 0 \tag{2}$$

However, we are less interested in how *large* the difference is, and more so how *often* B is larger than A. Let

$$\Delta_T(P, Q) = \Pr\left(B > A \;\middle|\; B \sim L(Q), A \sim L(P)\right)$$

where $0 \leq \Delta_T(P, Q) \leq 1$ represents how 'far' Q is from training sample T as compared to true distribution P. A more interpretable yet equally meaningful condition is

$$\Delta_T(P, Q) = \mathbb{E}_{\substack{A \sim L(P) \\ B \sim L(Q)}}[\mathbb{1}_{B > A}] \approx \frac{1}{2}$$

which guarantees Equation 2 if densities $L(P)$ and $L(Q)$ have the same shape, but are possibly mean-shifted.

If $\Delta_T(P, Q) << \frac{1}{2}$, Q is data-copying training set T, since samples from Q are systematically closer to T than are samples from P. However, even if $\Delta_T(P, Q) \geq \frac{1}{2}$, Q may still be data-copying T. As exhibited in **Figures 1b** and **1c**, a model Q may data-copy in one region and underfit in others. In this case, Q may be further from T than is P *globally*, but much closer to T *locally*. As such, we consider Q to be data-copying if it is overfit in any subspace $\mathcal{C} \subseteq \mathcal{X}$:

Definition 2.1. A generative model Q is *data-copying* training set T if, in some region $\mathcal{C} \subseteq \mathcal{X}$, it is systematically closer to T by distance metric $d : \mathcal{X} \to \mathbb{R}$ than are samples from P . Specifically, if

$$\Delta_T(P|_{\mathcal{C}}, Q|_{\mathcal{C}}) < \frac{1}{2}$$

This type of overfitting is orthogonal to the type of overfitting addressed by many previous works (Heusel et al., 2017; Sajjadi et al., 2018), which we call 'over-representation'. Here, Q overemphasizes some region of the instance space $\mathcal{C} \subseteq \mathcal{X}$, often a region of high density in the training set T.

Definition 2.2. A generative model Q is *over-representing* P in some region $\mathcal{C} \subseteq \mathcal{X}$, if the probability of drawing $Y \sim Q$ is much greater than it is of drawing $X \sim P$. Specifically, if

$$Q(\mathcal{C}) - P(\mathcal{C}) \gg 0$$

In this work we focus on data-copying, and provide a novel test to detect it.

2.2 A Global Data-Copying Test

We introduce our data-copying test in the global setting, when $\mathcal{C} = \mathcal{X}$. Here, we have a null hypothesis H_0 suggesting that Q may equal P:

$$H_0 : \Delta_T(P, Q) \;=\; \frac{1}{2} \tag{3}$$

There are well-established non-parametric tests for this hypothesis, such as the Mann-Whitney U test (Mann and Whitney, 1947). Let $A_i \sim L(P_n), B_j \sim L(Q_m)$ be samples of $L(P), L(Q)$ given by P_n, Q_m and their distances $d(X)$ to training set T. The U statistic estimates the probability in Equation 3 by measuring the number of all mn pairwise comparisons in which $B_j > A_i$. An efficient and simple method to gather and interpret this test is as follows:

1. Sort the $n+m$ values $L(P_n) \cup L(Q_m)$ such that each instance $l_i \in L(P_n), l_j \in L(Q_m)$ has rank $R(l_i), R(l_j)$, starting from rank 1, and ending with rank $n+m$. $L(P_n), L(Q_m)$ have no tied ranks with probability 1 assuming their distributions are continuous.

2. Calculate the rank-sum for $L(Q_m)$ denoted R_{Q_m}, and its U score denoted U_{Q_m}:

$$R_{Q_m} = \sum_{l_j \in L(Q_m)} R(l_j), \quad U_{Q_m} = R_{Q_m} - \frac{m(m+1)}{2}$$

   Consequently, $U_{Q_m} = \sum_{ij} \mathbb{1}_{B_j > A_i}$.

3. Under H_0, U_{Q_m} is approximately normally distributed with > 20 samples in both $L(Q_m)$ and $L(P_n)$, allowing for the following z-scored statistic:

$$Z_U\big(L(P_n), L(Q_m); T\big) = \frac{U_{Q_m} - \mu_U}{\sigma_U},$$
$$\mu_U = \frac{mn}{2}, \quad \sigma_U = \sqrt{\frac{mn(m+n+1)}{12}}$$

Z_U provides us a data-copying statistic with normalized expectation and variance under H_0. $Z_U \ll 0$ implies data-copying, $Z_U \gg 0$ implies underfitting. $Z_U < -5$ implies that if H_0 holds, Z_U is as likely as sampling a value < -5 from a standard normal. See Appendix 6.1 for consistency results.

This hypothesis test is a standard we can and should hold all generative models to. It is completely model agnostic and uses no estimate of likelihood. It only requires a meaningful distance metric, which is becoming common practice in the evaluation of mode-collapse and -dropping (Heusel et al., 2017; Sajjadi et al., 2018).

Additionally, the equal expectation condition of Equation 2 alone is almost sufficient to indicate a maximum likelihood Gaussian KDE model, like that in Equation 1, where the posterior probability that a random draw $x \sim q_\sigma(x)$ comes from the Gaussian component centered at training point t is

$$Q_\sigma(t|x) = \frac{\exp(-\|x-t\|^2/(2\sigma^2))}{\sum_{t' \in T} \exp(-\|x-t'\|^2/(2\sigma^2))}$$

Lemma 1. *For the kernel density estimator (1), the maximum-likehood choice of σ, namely the maximizer of $\mathbb{E}_{X\sim P}[\log q_\sigma(X)]$, satisfies*

$$\mathbb{E}_{X\sim P}\left[\sum_{t\in T} Q_\sigma(t|X)\|X-t\|^2\right] = \mathbb{E}_{Y\sim Q_\sigma}\left[\sum_{t\in T} Q_\sigma(t|Y)\|Y-t\|^2\right]$$

See Appendix 6.2 for proof. Unless σ is large, we know that for any given $x \in \mathcal{X}$, $\sum_{t\in T} Q_\sigma(t|x)\|x - t\|^2 \approx d(x) = \min_{t\in T}\|x-t\|^2$. So, enforcing that $\mathbb{E}_{X\sim P}[d(X)] = \mathbb{E}_{Y\sim Q}[d(Y)]$, and more loosely that $\mathbb{E}_{\substack{A\sim L(P)\\B\sim L(Q)}}[\mathbb{1}_{B>A}] = \frac{1}{2}$ provides an excellent non-parametric approach to selecting a Gaussian KDE, and ought to be enforced for any Q attempting to emulate P.

2.3 Handling Local Heterogeneity

As described in Section 2.1, the above global test can be fooled by generators Q which are very close to the training data in some regions of the instance space (overfitting) but very far from the training data in others (poor modeling).

To handle heterogeneity in practice, we introduce *local* versions of our earlier tests. Let Π denote any partition of the instance space $\mathcal{X}$, which can be constructed in any manner. In our experiments, for instance, we run the k-means algorithm on T, so that $|\Pi| = k$. As the number of training and test samples grows, we may increase k and thus the instance-space resolution of our test. Letting $L_\pi(D) = L(D|_\pi)$ be the distribution of distances-to-training-set within cell $\pi \in \Pi$, we probe each cell of the partition individually.

Data Copying To offer a summary statistic for data copying, we collect the z-scored Mann-Whitney U statistic, Z_U, described in Section 2.2 in each cell π. Let $P_n(\pi) = |\{x : x \in P_n, x \in \pi\}|/n$ denote the fraction of P_n points lying in cell π, and similarly for $Q_m(\pi)$. The Z_U test for cell π and training set T will then be denoted as $Z_U\big(L_\pi(P_n), L_\pi(Q_m); T\big)$, where $L_\pi(P_n) = \{d(x) : x \in P_n, x \in \pi\}$ and similarly for $L_\pi(Q_m)$. See **Figure 1c** for examples of these in-cell scores. For stability, we only measure data-copying for those cells significantly represented by Q, as determined by a threshold τ. Let Π_τ be the set of all cells in the partition Π for which $Q_m(\pi) \geq \tau$. Then, our summary statistic for data copying averages across all cells represented by Q:

$$C_T(P_n, Q_m) := \frac{\sum_{\pi \in \Pi_\tau} P_n(\pi) Z_U\big(L_\pi(P_n), L_\pi(Q_m); T\big)}{\sum_{\pi \in \Pi_\tau} P_n(\pi)}$$

Representation The above test will not catch a model that heavily over- or under-represents cells. For completeness, we make use of a simple representation test that is essentially used by Richardson and Weiss (2018), now with an independent test set instead of the training set.

With $n, m \geq 20$ in cell π, we may treat $Q_m(\pi), P_n(\pi)$ as Gaussian random variables. We then check the null hypothesis $H_0 : 0 = P(\pi) - Q(\pi)$. Assuming this null hypothesis, a simple z-test is:

$$Z_\pi = \frac{Q_m(\pi) - P_n(\pi)}{\sqrt{\widehat{p}(1-\widehat{p})\left(\frac{1}{n} + \frac{1}{m}\right)}}$$

where $\widehat{p} = \frac{nP_n(\pi) + mQ_m(\pi)}{n+m}$. We then report two values for a significance level $s = 0.05$: the number of significantly different cells ('bins') with $Z_\pi > s$ (NDB over-representing), and the number with $Z_\pi < -s$ (NDB under-representing).

Together, these summary statistics — C_T, NDB-over, NDB-under — establish a tension that encourages Q to broadly represent P without directly copying training set T.

3 Experiments

Having clarified what we mean by data-copying in theory, we turn our attention to observing data copying by generative models in practice. We leave representation test results for the appendix, since this behavior has been well studied in previous works. Specifically, we aim to answer the two following questions:

1. Are the existing tests that measure generative model overfitting able to capture data-copying?
2. When popular generative models range from over- to underfit, does our test indicate data-copying, and if so, to what degree?

Methods In all of the following experiments, we select a training dataset T with test split P_n, and a generative model Q producing sample Q_m. We perform k-means on T to determine partition Π, with the objective having a reasonable population of both T and P_n in each $\pi \in \Pi$. We set threshold τ, such that we are guaranteed to have at least 20 samples in each cell in order to validate the gaussian assumption of Z_π, Z_U.

We then select some parameter of Q that can tune the degree of over- or underfitting on training set T. For instance, the Gaussian KDE σ parameter will directly control the degree of data-copying by our definition, allowing us to sweep σ from low (complex, over-fit model) to high (simple, underfit model). For VAEs, we have no such parameter, and instead vary the model complexity from high (many units per layer) to low (few units per layer). We then probe for the degree of data-copying at each level of declining model complexity using the baseline and proposed methods, and record test responses. To observe the variance of each test, we record the average and 1-standard deviation of the test response across several trials of generating Q_m.

We embed all image samples into some latent space with meaningful L_2 distance to make $d(x)$ significant. While this is standard practice in evaluating generative models (Salimans et al., 2016; Sajjadi et al., 2018), these embeddings themselves might be overfit. To address this, we perform our experiments in three domains with three different kinds of embeddings (none, custom, and Inception Network Pool3 features).

3.1 Detecting data-copying

First, we investigate which of the existing generative model tests can detect explicit data-copying.

Baselines and Dataset Here, we probe the four of the methods described in our Related Work section, to see how they react to data-copying: two-sample NN (Lopez-Paz and Oquab, 2016), FID (Heusel et al., 2017), Binning-Based Evaluation (Richardson and Weiss, 2018), and Precision & Recall (Sajjadi et al., 2018), which are described in detail in Appendix 6.3.2. We run this test on the two-dimensional 'moons' dataset, as it affords us limitless training and test samples and requires no feature embedding (see Appendix 6.3.1 for an example). Note that, without an embedding, FID is simply the Frechét distance between two MLE normal distributions fit to T and Q_m. We use the same size generated and training sample for all methods, when $m < |T|$ (especially for large datasets and computationally burdensome samplers) we are forced to use an m-size training subsample $\widetilde{T}$ for running the two-sample NN test due to its constraint that $m = |T|$.

We compare against the canonical test of measuring the generalization gap (difference between training and test set likelihoods under the model) in Appendix 7. It is not a primary baseline since it cannot be used when the model likelihood is intractable.

We make Q a Gaussian KDE since it allows us to force explicit data-copying by setting σ very low. As $\sigma \to 0$, Q becomes a bootstrap sampler of the original training

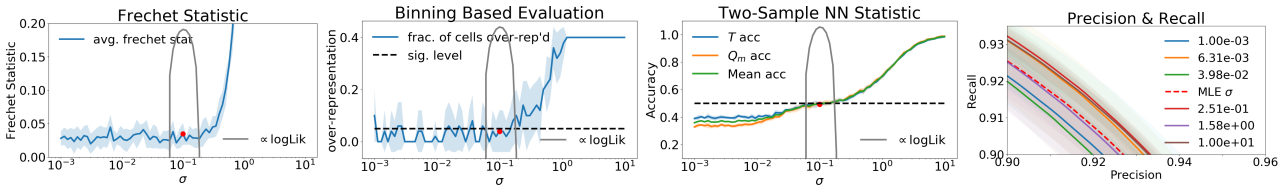

Figure 2: Response of four baseline test methods to data-copying of a Gaussian KDE on 'moons' dataset. Only the two-sample NN test **(c)** is able to detect data-copying KDE models as σ moves below σ_{MLE} (depicted as a red dot). The gray trace is proportional to the KDE's log-likelihood measured on a held-out validation set.

set. If a given test method can detect the level of data-copying by Q on T, it will provide a different response to a heavily over-fit KDE Q ($\sigma \ll \sigma_{\text{MLE}}$), a well-fit KDE Q ($\sigma \approx \sigma_{\text{MLE}}$), and an underfit KDE Q ($\sigma \gg \sigma_{\text{MLE}}$).

Figure 2 depicts how each baseline method responds to KDE Q models of varying degrees of data-copying, as Q ranges from data-copying ($\sigma = 0.001$) up to heavily underfit ($\sigma = 10$). The Frechét and Binning methods report effectively the same value for all $\sigma \leq \sigma_{\text{MLE}}$, indicating inability to detect data-copying. Similarly, the PR curves for different σ values are high variance and show no meaningful order with respect to σ.

The two-sample NN test does show a mild change in response as σ decreases below σ_{MLE}. This makes sense; as points in Q_m become closer to points in T, the two-sample NN accuracy should steadily drop to zero. The reason it does not drop to zero is due to the m subsampled training points, $\widetilde{T} \subset T$, needed to perform this test. As such, each training point $t \in T$ being copied by generated point $q \in Q_m$ is unlikely to be present in $\widetilde{T}$ during the test. This phenomenon is especially pronounced in some of the following settings.

The reason most of these tests fail to detect data-copying is because most existing methods focus on another type of overfitting: mode-collapse and -dropping, wherein entire modes of P are either forgotten or averaged together. However, if a model begins to data-copy, it is definitively overfitting *without* mode-collapsing.

Next, we will demonstrate our method on a variety of datasets, models, and embeddings. We will compare our method to the two-sample NN method in each setting, as it is the only baseline that responds to explicit data-copying.

3.2 Measuring degree of data-copying

We now aim to answer the second question raised at the beginning of this section: does $C_T(P_n, Q_m)$ detect and quantify data-copying? We focus on two types of generative model: Gaussian KDEs, and neural models.

3.2.1 KDE-based tests

While KDEs do not provide a reliable likelihood in high dimension (Theis et al., 2016), they do provide an informative first benchmark of the C_T statistic. KDEs allow us to directly force data-copying, and confirm the theoretical connection between the MLE KDE and $C_T \approx 0$ described in Lemma 1.

KDEs: 'moons' dataset Here, we repeat the experiment performed in Section 3.1, now including the C_T statistic for comparison. Refer to Appendix 6.3.1 for experimental details, and examples of the dataset.

Figures 3a and **3b** give a side-by-side depiction of C_T and the two-sample NN test accuracies across a range of KDE σ values. Think of C_T values as z-score standard deviations. We see that the C_T statistic in **Figure 3a** precisely identifies the MLE model when $C_T \approx 0$, and responds sharply to σ values above and below σ_{MLE}. The baseline in **Figure 3b** similarly identifies the MLE Q model when training accuracy ≈ 0.5, but is higher variance and less sensitive to changes in σ, especially for over-fit $\sigma \ll \sigma_{\text{MLE}}$. We will see in the next experiment, that this test breaks down for more complex datasets when $m \ll |T|$.

KDEs: MNIST Handwritten Digits We now extend the KDE test performed on the moons dataset to the significantly more complex MNIST handwritten digit dataset (LeCun and Cortes, 2010).

While it would be convenient to directly apply the KDE σ-sweeping tests discussed in the previous section, there are two primary barriers. The first is that KDE model relies on L_2 norms being perceptually meaningful, which is well understood not to be true in pixel space. The second problem is that of dimensionality: the 784-dimensional space of digits is far too high for a KDE to be even remotely efficient at interpolating the space.

To handle these issues, we first embed each image, $x \in \mathcal{X}$, to a perceptually meaningful 64-dimensional latent code, $z \in \mathcal{Z}$. We achieve this by training a convolutional autoencoder with a VGGnet perceptual

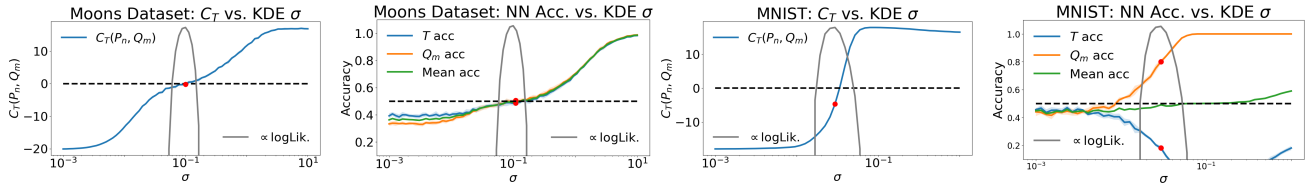

Figure 3: $C_T(P_n, Q_m)$ vs. NN baseline and generalization gap on moons and MNIST digits datasets. **(a,b)** compare the two tests on the moons dataset. **(c,d)** compare the two tests on MNIST. In both data settings, the C_T statistic is far more sensitive to the data-copying regime $\sigma \ll \sigma_{\text{MLE}}$ than the NN baseline. It is more sensitive to underfitting $\sigma \gg \sigma_{\text{MLE}}$ than the generalization gap test. The red dot denotes σ_{MLE}, and the gray trace is proportional to the KDE's log-likelihood measured on a held-out validation set.

loss produced by Zhang et al. (2018) (see Appendix 6.3.3 for more detail). Surely, even in the lower 64-dimensional space, the KDE will suffer some from the curse of dimensionality. We are not promoting this method as a powerful generative model, but rather as an instructive tool for probing a test's response to data-copying in the image domain.

Figure 3c shows how $C_T(P_n, Q_m)$ reacts decisively to over- and underfitting. It falsely determines the MLE σ value as slightly over-fit. However, the region of where C_T transitions from over- to underfit (say $-13 \leq C_T \leq 13$) is relatively tight and includes the MLE σ.

Meanwhile, **Figure 3d** shows how — with the generated sample smaller than the training sample, $m \ll |T|$ — the two-sample NN baseline provides no meaningful estimate of data-copying. In fact, the most data-copying models with low σ achieve the best scores closest to 0.5. Again, we are forced to use the m-subsampled $\widetilde{T} \subset T$, and most instances of data copying are completely missed. C_T has no such restriction.

These results are promising, and demonstrate the reliability of this hypothesis testing approach to probing for data-copying across different data domains. In the next section, we explore how these tests perform on more sophisticated, non-KDE models.

3.3 Neural Model Tests

Gaussian KDE's may have nice theoretical properties, but are relatively ineffective in high-dimensional settings, precluding domains like images. As such, we also demonstrate our experiments on more practical neural models trained on higher dimensional image datasets (MNIST and ImageNet), with the goal of observing whether the C_T statistic indicates data-copying as these models range from over- to underfit.

MNIST VAE Here, we employ our data-copying test, $C_T(P_n, Q_m)$, on a range of VAEs of varying complexity trained on the MNIST handwritten digit dataset. Experimental and theoretical findings have suggested that VAE samplers — under certain assumptions — simply produce convex combinations of training set samples (Bozkurt et al., 2018). In generating an out-of-distribution sample, an overly complex VAE effectively reproduces nearest-neighbor training samples. Our findings appear to corroborate this. We vary model complexity by increasing the width (neurons per layer) in a three-layer VAE (see Appendix 6.3.3 for details). As an embedding, we pass all samples through the the convolutional autoencoder of Section 3.2.1, and collect statistics in this 64-dimensional space.

Figures 4a and **4b** compare the C_T statistic to the NN accuracy baseline . C_T behaves as it did in the previous sections: more complex models over-fit, forcing $C_T \ll 0$, and less complex models underfit forcing it $\gg 0$. We note that the range of C_T values is far less dramatic, which is to be expected since the KDEs were forced to explicitly data-copy. As likelihood is not available for VAEs, we compute each model's ELBO on a 10,000 sample held out validation set, and plot it in gray. We observe that the ELBO spikes for models with C_T near 0.

The NN baseline in **Figure 4b** is less interpretable, and fails to capture the overfitting trend as C_T does. While all three test accuracies still follow the upward-sloping trend of **Figure 3b**, they do not indicate where the highest validation set ELBO is. Furthermore, the NN accuracy statistics are shifted upward when compared to the results of the previous section: all NN accuracies are above 0.5 for all latent dimensions. This is problematic. A test statistic's absolute score ought to bear significance between very different data and model domains like KDEs and VAEs.

ImageNet GAN Finally, we scale our experiments up to a more practical image domain. We gather our test statistics on a state of the art conditional GAN, '*BigGan*' (Brock et al., 2018), trained on the Imagenet 12 dataset (Russakovsky et al., 2015). Conditioning on an input code, this GAN will generate one of 1000 different Imagenet classes. We run our experiments separately on three classes: 'coffee', 'soap bubble', and 'schooner'. All generated, test, and training images are

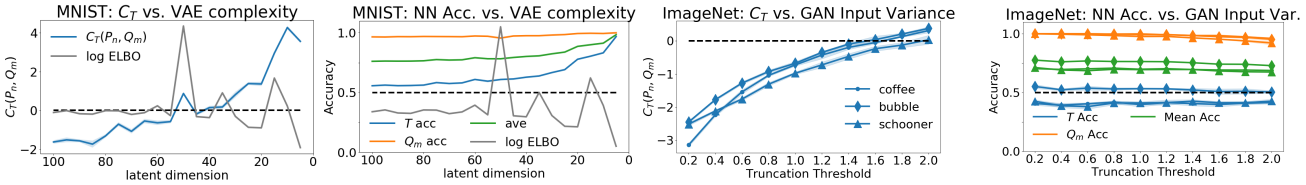

(a) **(b)** **(c)** **(d)**

Figure 4: Neural model data-copying: figures **(a)** and **(c)** demonstrate the C_T statistic identifying data-copying in an MNIST VAE and ImageNet GAN as they range from heavily over-fit to underfit. **(b)** and **(d)** demonstrate the relative insensitivity of the NN baseline to this overfitting. (Note, the markers for **(d)** apply to the traces of **(e)**)

(a) Data-copied cells; top: $Z_U = -1.46$, bottom: $Z_U = -1.00$

(b) Underfit cells; top: $Z_U = +1.40$, bottom: $Z_U = +0.71$

Figure 5: Data-copied and underfit cells of ImageNet12 'coffee' and 'soap bubble' instance spaces (trunc. threshold = 2). In each 14-figure strip, the top row provides a random series of training samples from the cell, and the bottom row provides a random series of generated samples from the cell. **(a)** Data-copied cells. **(a), top**: Random training and generated samples from a $Z_U = -1.46$ cell of the coffee instance space. **(a), bottom**: Random training and generated samples from a $Z_U = -1.00$ cell of the bubble instance space. **(b)** Underfit cells. **(b), top**: Random training and generated samples from a $Z_U = +1.40$ cell of the coffee instance space. **(b), bottom**: Random training and generated samples from a $Z_U = +0.71$ cell of the bubble instance space.

embedded to a 64-dimensional space by first gathering the 2048-dimensional features of an InceptionV3 network 'Pool3' layer, and then projecting them onto the 64 principal components of the training embeddings. Appendix 6.3.4 has more details.

Being limited to one pre-trained model, we increase model variance ('truncation threshold') instead of decreasing model complexity. As proposed by *BigGan*'s authors, all standard normal input samples outside of this truncation threshold are resampled. The authors suggest that lower truncation thresholds, by only producing samples at the mode of the input, output higher quality samples at the cost of variety, as determined by Inception Score (IS). Similarly, the FID score finds suitable variety until truncation approaches zero.

As depicted in **Figure 4c**, the C_T statistic remains well below zero until the truncation threshold is nearly maximized, indicating that Q produces samples closer to the training set than real samples tend to be. While FID finds that *in aggregate* the distributions are roughly similar, a closer look suggests that Q allocates too much probability mass near the training samples.

Meanwhile, the two-sample NN baseline in **Figure 4d** hardly reacts to changes in truncation, even though the generated and training sets are the same size, $m = |T|$. Across all truncation values, the training sample NN accuracy remains around 0.5, not quite implying over- or underfitting.

A useful feature of the C_T statistic is that one can examine the Z_U scores it is composed of to see which of the cells $\pi \in \Pi_\tau$ are or are not copying. **Figure 5** shows the samples of over- and underfit cells $\pi \in \Pi$ for two of the three classes. For both 'coffee' and 'bubble' classes, the underfit cells are more diverse than the data-copied cells. While it might seem reasonable that these generated samples are further from nearest neighbors in more diverse clusters, keep in mind that the $Z_U > 0$ statistic indicates that they are further from training neighbors than test set samples are. For instance, the people depicted in underfit 'bubbles' cell are highly distorted.

4 Conclusion

In this work, we have formalized *data-copying*: an under-explored failure mode of generative model overfitting. We have provided preliminary tests for measuring data-copying and experiments indicating its presence in a broad class of generative models. In future work, we plan to establish more theoretical properties of data-copying, convergence guarantees of these tests, and experiments with different model parameters.

5 Acknowledgements

We thank Rich Zemel for pointing us to Xu et al. (2018), which was the starting point of this work. Thanks to Arthur Gretton and Ruslan Salakhutdinov for pointers to prior work, and Philip Isola and Christian Szegedy for helpful advice. Finally, KC and CM would like to thank N00014-16-1-261, UC Lab Fees under LFR 18-548554 and NSF IIS 1617157 for research support.

References

Wacha Bounliphone, Eugene Belilovsky, Matthew B. Blaschko, Ioannis Antonoglou, and Arthur Gretton. A test of relative similarity for model selection in generative models. In *4th International Conference on Learning Representations, ICLR 2016, San Juan, Puerto Rico, May 2-4, 2016, Conference Track Proceedings*, 2016. URL http://arxiv.org/abs/1511.04581.

Alican Bozkurt, Babak Esmaeili, Dana H Brooks, Jennifer G Dy, and Jan-Willem van de Meent. Can vaes generate novel examples? 2018.

Andrew Brock, Jeff Donahue, and Karen Simonyan. Large scale gan training for high fidelity natural image synthesis, 2018.

Tong Che, Yanran Li, Athul Paul Jacob, Yoshua Bengio, and Wenjie Li. Mode regularized generative adversarial networks. *CoRR*, abs/1612.02136, 2016. URL http://arxiv.org/abs/1612.02136.

Cristóbal Esteban, Stephanie L Hyland, and Gunnar Rätsch. Real-valued (medical) time series generation with recurrent conditional gans. *arXiv preprint arXiv:1706.02633*, 2017.

Ian Goodfellow, Jean Pouget-Abadie, Mehdi Mirza, Bing Xu, David Warde-Farley, Sherjil Ozair, Aaron Courville, and Yoshua Bengio. Generative adversarial nets. In *Advances in neural information processing systems*, pages 2672–2680, 2014.

Ishaan Gulrajani, Colin Raffel, and Luke Metz. Towards GAN benchmarks which require generalization. *CoRR*, abs/2001.03653, 2020. URL https://arxiv.org/abs/2001.03653.

Martin Heusel, Hubert Ramsauer, Thomas Unterthiner, Bernhard Nessler, and Sepp Hochreiter. Gans trained by a two time-scale update rule converge to a local nash equilibrium. 2017.

Diederik P Kingma and Max Welling. Auto-encoding variational bayes. *arXiv preprint arXiv:1312.6114*, 2013.

Tuomas Kynkäänniemi, Tero Karras, Samuli Laine, Jaakko Lehtinen, and Timo Aila. Improved precision and recall metric for assessing generative models. Advances in Neural Information Processing Systems 33 (NIPS 2019), 2019.

Yann LeCun and Corinna Cortes. MNIST handwritten digit database. 2010. URL http://yann.lecun.com/exdb/mnist/.

David Lopez-Paz and Maxime Oquab. Revisiting classifier two-sample tests. *arXiv preprint arXiv:1610.06545*, 2016.

Henry B Mann and Donald R Whitney. On a test of whether one of two random variables is stochastically larger than the other. *The annals of mathematical statistics*, pages 50–60, 1947.

Eitan Richardson and Yair Weiss. On gans and gmms. In *Advances in Neural Information Processing Systems*, pages 5847–5858, 2018.

Olga Russakovsky, Jia Deng, Hao Su, Jonathan Krause, Sanjeev Satheesh, Sean Ma, Zhiheng Huang, Andrej Karpathy, Aditya Khosla, Michael Bernstein, Alexander C. Berg, and Li Fei-Fei. ImageNet Large Scale Visual Recognition Challenge. *International Journal of Computer Vision (IJCV)*, 115(3):211–252, 2015. doi: 10.1007/s11263-015-0816-y.

Mehdi S. M. Sajjadi, Olivier Bachem, Mario Lucic, Olivier Bousquet, and Sylvain Gelly. Assessing generative models via precision and recall. Advances in Neural Information Processing Systems 31 (NIPS 2017), 2018.

Tim Salimans, Ian Goodfellow, Wojciech Zaremba, Vicki Cheung, Alec Radford, and Xi Chen. Improved techniques for training gans. In *Advances in neural information processing systems*, pages 2234–2242, 2016.

Dougal J. Sutherland, Hsiao-Yu Fish Tung, Heiko Strathmann, Soumyajit De, Aaditya Ramdas, Alexander J. Smola, and Arthur Gretton. Generative models and model criticism via optimized maximum mean discrepancy. *CoRR*, abs/1611.04488, 2016. URL http://arxiv.org/abs/1611.04488.

Lucas Theis, Aäron van den Oord, and Matthias Bethge. A note on the evaluation of generative models. In *4th International Conference on Learning Representations, ICLR 2016, San Juan, Puerto Rico, May 2-4, 2016, Conference Track Proceedings*, 2016. URL http://arxiv.org/abs/1511.01844.

Ryan Webster, Julien Rabin, Loïc Simon, and Frédéric Jurie. Detecting overfitting of deep generative networks via latent recovery. In *IEEE Conference on Computer Vision and Pattern Recognition, CVPR 2019, Long Beach, CA, USA, June 16-20, 2019*, pages 11273–11282. Computer Vision Foundation / IEEE, 2019. doi: 10.1109/CVPR.2019.01153. URL http://openaccess.thecvf.com/content_CVPR_

2019/html/Webster_Detecting_Overfitting_of_Deep_Generative_Networks_via_Latent_Recovery_CVPR_2019_paper.html.

Yuhuai Wu, Yuri Burda, Ruslan Salakhutdinov, and Roger B. Grosse. On the quantitative analysis of decoder-based generative models. In *5th International Conference on Learning Representations, ICLR 2017, Toulon, France, April 24-26, 2017, Conference Track Proceedings*, 2017. URL https://openreview.net/forum?id=B1M8JF9xx.

Qiantong Xu, Gao Huang, Yang Yuan, Chuan Guo, Yu Sun, Felix Wu, and Kilian Weinberger. An empirical study on evaluation metrics of generative adversarial networks. *arXiv preprint arXiv:1806.07755*, 2018.

Richard Zhang, Phillip Isola, Alexei A Efros, Eli Shechtman, and Oliver Wang. The unreasonable effectiveness of deep features as a perceptual metric. In *CVPR*, 2018.

6 Appendix

6.1 Performance Guarantees

Even when H_0 does not hold, U_{Q_m} has desirable properties. First and foremost, $\frac{1}{mn}U_{Q_m}$ is a consistent estimator of the quantity of interest, $\Delta_T(P,Q)$:

Theorem 2. *For true distribution P, model distribution Q, and distance metric $d : \mathcal{X} \to \mathbb{R}$, the estimator $\frac{1}{mn}U_{Q_m} \to_P \Delta(P,Q)$ according to the concentration inequality*

$$\Pr\big(\big|\frac{1}{mn}U_{Q_m} - \Delta(P,Q)\big| \geq t\big) \leq \exp\bigg(-\frac{2t^2 mn}{m+n}\bigg)$$

Proof. We establish consistency using the following nifty lemma

Lemma 3. *(Bounded Differences Inequality) Suppose $X_1, \ldots, X_n \in \mathcal{X}$ are independent, and $f : \mathcal{X}^n \to \mathbb{R}$. Let $c_1, \ldots, c_n$ satisfy*

$$\sup_{x_1,\ldots,x_n,x_i'} \big|f(x_1,\ldots,x_i,\ldots,x_n) - f(x_1,\ldots,x_i',\ldots,x_n)\big| \leq c_i$$

for $i = 1, \ldots, n$. Then we have for any $t > 0$

$$\Pr\big(\big|f - \mathbb{E}[f]\big| \geq t\big) \leq \exp\bigg(\frac{-2t^2}{\sum_{i=1}^n c_i^2}\bigg) \qquad (4)$$

This directly equips us to prove the Theorem.

It is relatively straightforward to apply Lemma 3 to the normalized $\overline{U} = \frac{1}{mn}U_{Q_m}$. First, think of it as a function of m independent samples of $X \sim Q$ and n independent samples of $Y \sim P$, $\overline{U}(X_1,\ldots,X_m,Y_1,\ldots,Y_n) = \frac{1}{mn}\sum_{ij} \mathbb{1}_{d(X_i)>d(Y_j)}$

$$\overline{U} : (\mathbb{R}^d)^{mn} \to \mathbb{R}$$

Let b_i bound the change in $\overline{U}$ after substituting any X_i with X_i', and c_j bound the change in $\overline{U}$ after substituting any Y_j with Y_j'. Specifically

$$\sup_{x_1,\ldots,x_m,y_1,\ldots,y_n,\ x_i'} \big|\overline{U}(x_1,\ldots,x_i,\ldots,x_m,y_1,\ldots,y_n) - \overline{U}(x_1,\ldots,x_i',\ldots,x_m,y_1,\ldots,y_n)\big| \leq b_i$$

$$\sup_{x_1,\ldots,x_m,y_1,\ldots,y_n,\ y_j'} \big|\overline{U}(x_1,\ldots,x_m,y_1,\ldots,y_j,\ldots y_n) - \overline{U}(x_1,\ldots,x_m,y_1,\ldots,y_j',\ldots y_n)\big| \leq c_i$$

We then know that $b_i = \frac{n}{mn} = \frac{1}{m}$ for all i, with equality when $d(x_i') < d(y_j) < d(x_i)$ for all $j \in [n]$. In this case, substituting x_i with x_i' flips n of the indicator comparisons in $\overline{U}$ from 1 to 0, and is then normalized by mn. By a similar argument, $c_j = \frac{m}{nm} = \frac{1}{n}$ for all j.

Equipped with b_i and c_j, we may simply substitute into Equation 4 of the Bounded Differences Inequality, giving us

$$\begin{aligned}\Pr\big(\big|\overline{U} - \mathbb{E}[\overline{U}]\big| \geq t\big) &= \Pr\big(\big|\frac{1}{mn}U_{Q_m} - \Delta(\mu_p,\mu_q)\big| \geq t\big)\\ &\leq \exp\bigg(\frac{-2t^2}{\sum_{i=1}^m b_i^2 + \sum_{j=1}^n c_j^2}\bigg)\\ &= \exp\bigg(\frac{-2t^2}{\sum_{i=1}^m \frac{1}{m^2} + \sum_{j=1}^n \frac{1}{n^2}}\bigg)\\ &= \exp\bigg(\frac{-2t^2}{\frac{1}{m}+\frac{1}{n}}\bigg) = \exp\bigg(\frac{-2t^2 mn}{m+n}\bigg)\end{aligned}$$

∎

Furthermore, when the model distribution Q actually matches the true distribution P, under modest assumptions we can expect $\frac{1}{mn}U_{Q_m}$ to be near $\frac{1}{2}$:

Theorem 4. *When $Q = P$, and the corresponding distance distribution $L(Q) = L(P)$ is non-atomic,*

$$\mathbb{E}\Big[\frac{1}{mn}U_{Q_m}\Big] = \frac{1}{2} \quad \textit{and} \quad \mathbb{E}[Z_U] = 0$$

Proof. For random variables $A \sim L(P)$ and $B \sim L(P)$, we can partition the event space of $A \times B$ into three disjoint events:

$$\begin{aligned}&\Pr(A > B) + \Pr(A < B)\\ &\qquad + \Pr(A = B) = 1\end{aligned}$$

Since $Q = P$, the first two events have equal probability, $\Pr(A > B) = \Pr(A < B)$, so

$$2\Pr(A > B) + \Pr(A = B) = 1$$

And since the distributions of A and B are non-atomic (i.e. $\Pr\big(B = b\big) = 0, \quad \forall\, b \in \mathbb{R}$) we have that $\Pr(A = B) = 0$, and thus

$$\begin{aligned}2\Pr(A > B) &= 1\\ \Pr(A > B) = \Delta(P,Q) &= \frac{1}{2}\end{aligned}$$

∎

6.2 Proof of Lemma 1

Lemma 1 *For the kernel density estimator (1), the maximum-likehood choice of σ, namely the maximizer*

of $\mathbb{E}_{X\sim P}[\log q_\sigma(X)]$*, satisfies*

$$\mathbb{E}_{X\sim P}\left[\sum_{t\in T} Q_\sigma(t|X)\|X-t\|^2\right] = \mathbb{E}_{Y\sim Q_\sigma}\left[\sum_{t\in T} Q_\sigma(t|Y)\|Y-t\|^2\right]$$

Proof. We have

$$\begin{aligned}&\mathbb{E}_{X\sim P}\left[\ln q_\sigma(X)\right]\\ &= \mathbb{E}_{X\sim P}\left[-\ln((2\pi)^{k/2}|T|\sigma^k) + \ln\sum_{t\in T}\exp\left(-\frac{\|x-t\|^2}{2\sigma^2}\right)\right]\\ &= \text{constant} - k\ln\sigma + \mathbb{E}_{X\sim P}\left[\ln\sum_{t\in T}\exp\left(-\frac{\|x-t\|^2}{2\sigma^2}\right)\right]\end{aligned}$$

Setting the derivative of this to zero and simplifying, we find that the maximum-likelihood σ satisfies

$$\sigma^2 = \frac{1}{k}\,\mathbb{E}_{X\sim P}\left[\sum_{t\in T} Q_\sigma(t|X)\|X-t\|^2\right]. \qquad (5)$$

Now, interpreting Q_σ as a mixture of $|T|$ Gaussians, and using the notation $t \in_R T$ to mean that t is chosen uniformly at random from T, we have

$$\begin{aligned}&\mathbb{E}_{Y\sim Q_\sigma}\left[\sum_{t\in T} Q_\sigma(t|Y)\|Y-t\|^2\right]\\ &= \mathbb{E}_{t\in_R T}\mathbb{E}_{Y\sim N(t,\sigma^2 I_k)}\left[\|Y-t\|^2\right] = k\sigma^2.\end{aligned}$$

Combining this with (5) yields the lemma. ∎

6.3 Procedural Details of Experiments

6.3.1 Moons Dataset, and Gaussian KDE

moons dataset 'Moons' is a synthetic dataset consisting of two curved interlocking manifolds with added configurable noise. We chose to use this dataset as a proof of concept because it is low dimensional, and thus KDE friendly and easy to visualize, and we may have unlimited train, test, and validation samples.

Gaussian KDE We use a Gaussian KDE as our preliminary generative model Q because its likelihood is theoretically related to our non-parametric test. Perhaps more importantly, it is trivial to control the degree of data-copying with the bandwidth parameter σ. **Figures 6b, 6c, 6d** provide contour plots of of a Gaussian KDE Q trained on the moons dataset with progressively larger σ. With $\sigma = 0.01$, Q will effectively resample the training set. $\sigma = 0.13$ is nearly the MLE model. With $\sigma = 0.5$, the KDE struggles to capture the unique definition of T.

6.3.2 Moons Experiments

Our experiments that examined whether several baseline tests could detect data-copying (Section 3.1), and our first test of our own metric (Section 3.2.1) use the moons dataset. In both of these, we fix a training sample, T of 2000 points, a test sample P_n of 1000 points, and a generated sample Q_m of 1000 points. We regenerate Q_m 10 times, and report the average statistic across these trials along with a single standard deviation. If the standard deviation buffer along the line is not visible, it is because the standard deviation is relatively small. We artificially set the constraint that $m, n \ll |T|$, as is true for big natural datasets, and more elaborate models that are computationally burdensome to sample from.

Section 3.1 Methods Here are the routines we used for the four baseline tests:

- **Frechét Inception Distance (FID)** (Heusel et al., 2017): Normally, this test is run on two samples of images (T and Q_m) that are first embedded into a perceptually meaningful latent space using a discriminative neural net, like the Inception Network. By 'meaningful' we mean points that are closer together are more perceptually alike to the human eye. Unlike images in pixel space, the samples of the moons dataset require no embedding, so we run the Frechét test directly on the samples.

  First, we fit two MLE Gaussians: $\mathcal{N}(\mu_T, \Sigma_T)$ to T, and $\mathcal{N}(\mu_Q, \Sigma_Q)$ to Q_m, by collecting their respective MLE mean and covariance parameters. The statistic reported is the Frechét distance between these two Gaussians, denoted $\mathrm{Fr}(\bullet, \bullet)$, which for Gaussians has a closed form:

  $$\begin{aligned}&\mathrm{Fr}\big(\mathcal{N}(\mu_T, \Sigma_T), \mathcal{N}(\mu_Q, \Sigma_Q)\big) =\\ &\quad \|\mu_T - \mu_Q\| + \mathbf{Tr}\big(\Sigma_T - \Sigma_Q - 2(\Sigma_T\Sigma_Q)^{1/2}\big)\end{aligned}$$

  Naturally, if Q is data-copying T, its MLE mean and covariance will be nearly identical, rendering this test ineffective for capturing this kind of overfitting.

- **Binning Based Evaluation** (Richardson and Weiss, 2018): This test, takes a hypothesis testing approach for evaluating mode collapse and deletion. The test bears much similarity to the test described in Section 2.3. The basic idea is as follows. Split the training set into partition Π using k-means; the number of samples falling into each bin is approximately normally distributed if it has $>$20 samples. Check the null hypothesis that the normal distribution of the fraction of the training

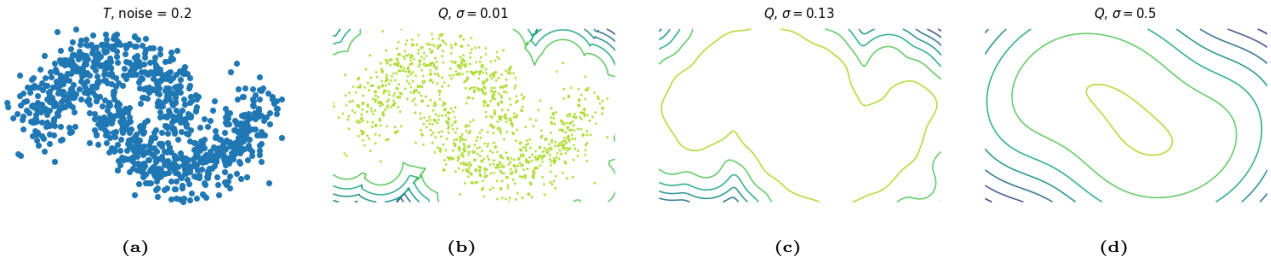

Figure 6: Contour plots of KDE fit on T: a) training T sample, b) over-fit 'data copying' KDE, c) max likelihood KDE, d) underfit KDE

set in bin π, $T(\pi)$, equals the normal distribution of the fraction of the generated set in bin π, $Q_m(\pi)$. Specifically:

$$Z_\pi = \frac{Q_m(\pi) - T(\pi)}{\sqrt{\widehat{p}(1-\widehat{p})\left(\frac{1}{|T|} + \frac{1}{m}\right)}}$$

where $\widehat{p} = \frac{|T|T(\pi) + mQ_m(\pi)}{|T|+m}$. We then perform a one-sided hypothesis test, and compute the number of positive Z_π values that are greater than the significance level of 0.05. We call this the number of statistically different bins or NDB. The NDB/k ought to equal the significance level if $P = Q$.

- **Two-Sample Nearest-Neighbor** (Lopez-Paz and Oquab, 2016): In this test — our primary baseline — we report the three LOO NN values discussed in Xu et al. (2018). The generated sample Q_m and training sample (subsampled to have equal size, m), $\widetilde{T} \subseteq T$, are joined together create sample $S = \widetilde{T} \cup Q_m$ of size $2m$, with training samples labeled '1' and test samples labeled '0'. One then fits a 1-Nearest-Neighbor classifier to S, and reports the accuracy in predicting the training samples ('1's), the accuracy in predicting the generated samples ('0's), and the average.

  One can expect that — when Q collapses to a few mode centers of T — the training accuracy is low, and the generated accuracy is high, thus indicating over-representation. Additionally, one could imagine that when the training and generated accuracies are near 0, we have extreme data-copying. However, as explained in Experiments section, when we are forced to subsample T, it is unlikely that a given copied training point $t \in T$ is used in the test, thus making the test result unclear.

- **Precision and Recall** (Sajjadi et al., 2018): This method offers a clever technique for scaling classical precision and recall statistics to high dimensional, complex spaces. First, all samples are embedded to Inception Network Pool3 features. Then, the author's use the following insight: for distribution's Q and P, the precision and recall curve is approximately given by the set of points:

$$\widehat{\text{PRD}}(Q, P) = \{(\alpha(\lambda), \beta(\lambda) | \lambda \in \Lambda\}$$

where

$$\Lambda = \{\tan\left(\frac{i}{r+1}\frac{\pi}{2}\right) | i \in [r]\}$$
$$\alpha(\lambda) = \sum_{\pi \in \Pi} \min\left(\lambda P(\pi), Q(\pi)\right)$$
$$\beta(\lambda) = \sum_{\pi \in \Pi} \min\left(P(\pi), \frac{Q(\pi)}{\lambda}\right)$$

and where r is the 'resolution' of the curve, the set Π is a partition of the instance space and $P(\pi), Q(\pi)$ are the fraction of samples falling in cell π. Π is determined by running k-means on the combination of the training and generated sets. In our tests here, we set $k = 5$, and report the average PRD curve measured over 10 k-means clusterings (and then re-run 10 times for 10 separate trials of Q_m).

6.3.3 MNIST Experiments

The experiments of Sections 3.2.1 and 3.3 use the MNIST digit dataset (LeCun and Cortes, 2010). We use a training sample, T, of size $|T| = 50,000$, a test sample P_n of size $n = 10,000$, a validation sample V_l of $l = 10,000$, and create generated samples of size $m = 10,000$.

Here, for a meaningful distance metric, we create a custom embedding using a convolutional autoencoder trained using a VGG perceptual loss proposed by Zhang et al. (2018). The encoder and decoder each have four convolutional layers using batch normalization, two linear layers using dropout, and two max pool layers. The autoencoder is trained for 100 epochs with a batch size of 128 and Adam optimizer with learning rate 0.001. For each training sample $t \in \mathbb{R}^{784}$, the encoder compresses to $z \in \mathbb{R}^{64}$, and decoder expands back up to $\widehat{t} \in \mathbb{R}^{784}$. Our loss is then

$$L(t, \widehat{t}) = \gamma(t, \widehat{t}) + \lambda \max\{\|z\|_2^2 - 1, 0\}$$

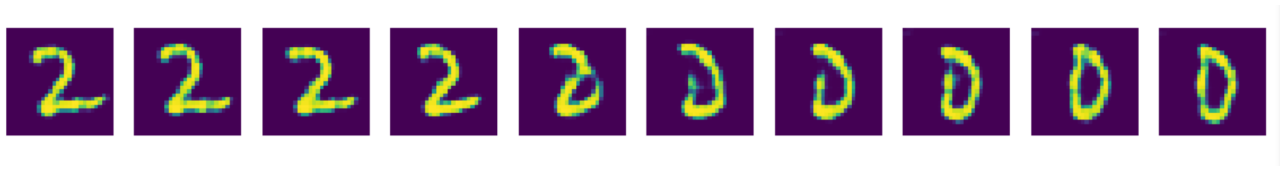

Figure 7: Interpolating between two points in the latent space to demonstrate L_2 perceptual significance

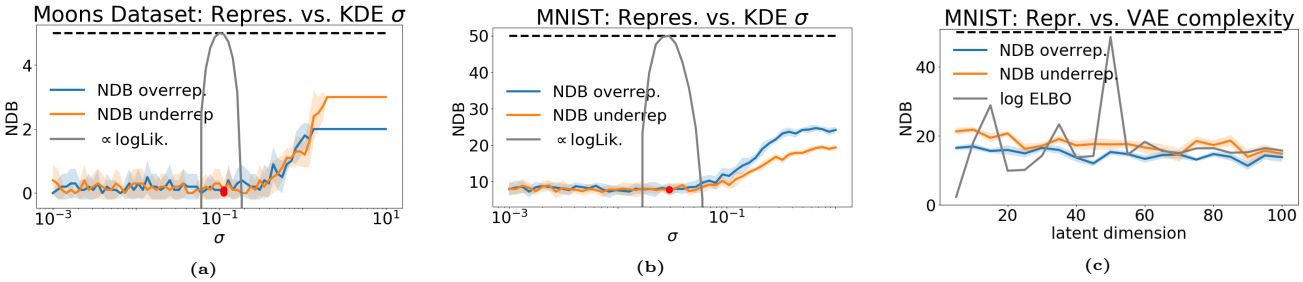

Figure 8: Number of statistically different bins, both those over and under the significance level of 0.05. The black dotted line indicates the total number of cells or 'bins'. **(a,b)** KDEs tend to start misrepresenting with $\sigma \gg \sigma_{\text{MLE}}$, which makes sense as they become less and less dependent on training set. **(c)** it makes sense that the VAE over- and under-represents across all latent dimensions due to its reverse KL loss. There is slightly worse over- and under-representation for simple models with low latent dimension.

where $\gamma(\bullet, \bullet)$ is the VGG perceptual loss, and $\lambda \max\{\|z\|_2^2 - 1, 0\}$ provides a linear hinge loss outside of a unit L_2 ball. The hinge loss encourages the encoder to learn a latent representation within a bounded domain, hopefully augmenting its ability to interpolate between samples. It is worth noting that the perceptual loss is not trained on MNIST, and hopefully uses agnostic features that help keep us from overfitting. We opt to use a standard autoencoder instead of a stochastic autoencoder like a VAE, because we want to be able to exactly data-copy the training set T. Thus, we want the encoder to create a near-exact encoding and decoding of the training samples specifically. **Figure 7** provides an example of linearly spaced steps between two training samples. While not perfect, we observe that half-way between the '2' and the '0' is a sample that appears perceptually to be almost almost a '2' and almost a '0'. As such, we consider the distance metric $d(x)$ on this space used in our experiments to be meaningful.

KDE tests: In the MNIST KDE experiments, we fit each KDE Q on the 64-d latent representations of the training set T for several values of σ; we gather all statistical tests in this space, and effectively only decode to visaully inspect samples. We gather the average and standard deviation of each data point across 5 trials of generating Q_m. For the Two-Sample Nearest-Neighbor test, it is computationally intense to compute the nearesnt neighbor in a 64-dimensional dataset of 20,000 points $\widetilde{T} \cup Q_m$ 20,000 times. To limit this, we average each of the training and generated NN accuracy over 500 training and generated samples. We find this acceptable, since the test results depicted in **Figure 3d** are relatively low variance.

VAE experiments: In the MNIST VAE experiments, we only use the 64-d autoencoder latent representation in computing the C_T and 1-NN test scores, and not at all in training. Here, we experiment with twenty standard, fully connected, VAEs using binary cross entropy reconstruction loss. The twenty models have three hidden layers and latent dimensions ranging from $d = 5$ to $d = 100$ in steps of 5. The number of neurons in intermediate layers is approximately twice the number of the layer beneath it, so for a latent space of 50-d, the encoder architecture is $784 \to 400 \to 200 \to 100 \to 50$, and the decoder architecture is the opposite.

To sample from a trained VAE, we sample from a standard normal with dimensionality equivalent to the VAEs latent dimension, and pass them through the VAE decoder to the 784-d image space. We then encode these generated images to the agnostic 64-d latent space of the perceptual autoencoder described at the beginning of the section, where L_2 distance is meaningful. We also encode the training sample T and test sample P_n to this space, and then run the C_T and two-sample NN tests. We again compute the nearest neighbor accuracies for 500 of the training and generated samples (the 1-NN classifier is fit on the 20,000 sample set $\widetilde{T} \cup Q_m$), which appears to be acceptable due to low test variance.

6.3.4 ImageNet Experiments

Here, we have chosen three of the one thousand ImageNet12 classes that 'BigGan' produces. To reiterate,

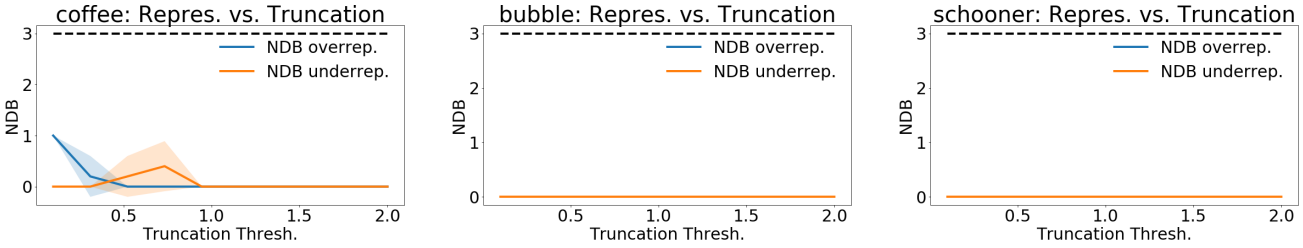

(a) (b) (c)

Figure 9: This GAN model produces relatively equal representation according to our clustering for all three classes. It makes sense that a low truncation level tends to over-represent for one class, as a lower truncation threshold causes less variance. Even though it places samples into all cells, some cells are data-copying much more aggressively than others.

(a) $Z_U = -1.05$ **(b)** $Z_U = +1.32$

Figure 10: Example of data-copied and underfit cell of ImageNet 'schooner' instance space, from 'BigGan' with trunc. threshold = 2. We note here, that — limited to only 50 training samples — the insufficient $k = 3$ clustering is perhaps not fine grain enough for this class. Notice that the generated samples falling into the underfit cell (mostly training images of either masts or fronts of boats) are hardly any different from those of the over-fit cell. They are likely on the boundary of the two cells. With that said, the samples of the data-copied cell **(a)** are certainly close to the training samples in this region.

a conditional GAN can output samples from a specific class by conditioning on a class code input. We acknowledge that conditional GANs combine features from many classes in ways not yet well understood, but treat the GAN of each class as a uniquely different generative model trained on the training samples from that class. So, for the 'coffee' class, we treat the GAN as a coffee generator Q, trained on the 1300 'coffee' class samples. For each class, we have 1300 training samples $|T|$, 2000 generated samples m, and 50 test samples n. Being atypically training sample starved ($m > |T|$), we subsample Q_m (not T!), to produce equal size samples for the two-sample NN test. As such, all training samples used are in the combined set S. We also note that the 50 test samples provided in each class is highly limiting, only allowing us to split the instance space into about three cells and keep a reasonable number of test samples in each cell. As the number of test samples grows, so can the number of cells and the resolution of the partition. **Figure 10** provides an example of where this clustering might be limited; the generated samples of the underfit cell seem hardly any different from those of the over-fit cell. A finer-grain partition is likely needed here. However, the data-copied cell to the left does appear to be very close to the training set, potentially too close according to Z_U.

In performing these experiments, we gather the $C_T(P_n, Q_m)$ statistic for a given class of images. In an attempt to embed the images into a lower dimensional latent space with L_2 significance, we pass each image through an InceptionV3 network and gather the 2048-dimension feature embeddings after the final average pooling layer (Pool3). We then project all inception-space images (T, P_n, Q_m) onto the 64 principal components of the training set embeddings. Finally, we use k-means to partition the points of each sample into one of $k = 3$ cells. The number of cells is limited by the 50 test images available per class. Any more cells would strain the Central Limit Theorem assumption in computing Z_U. Finally, we gather the C_T and two-sample NN baseline statistics on this 64-d space.

6.4 Comparison with three-sample Kernel-MMD:

Another three-sample test not shown in the main body of this work is the three-sample kernel MMD test introduced by Bounliphone et al. (2016) intended more for model comparison than for checking model overfitting. For samples $X \sim P$ and $Y \sim Q$, we can estimate the squared kernel MMD between P and Q under kernel k by empirically estimating

$$\text{MMD}^2(P, Q)$$
$$= \mathbb{E}_{x,x' \sim P}[k(x, x')] - 2\mathbb{E}_{x \sim P, y \sim Q}[k(x, y)] + \mathbb{E}_{y,y' \sim Q}[k(y, y')]$$

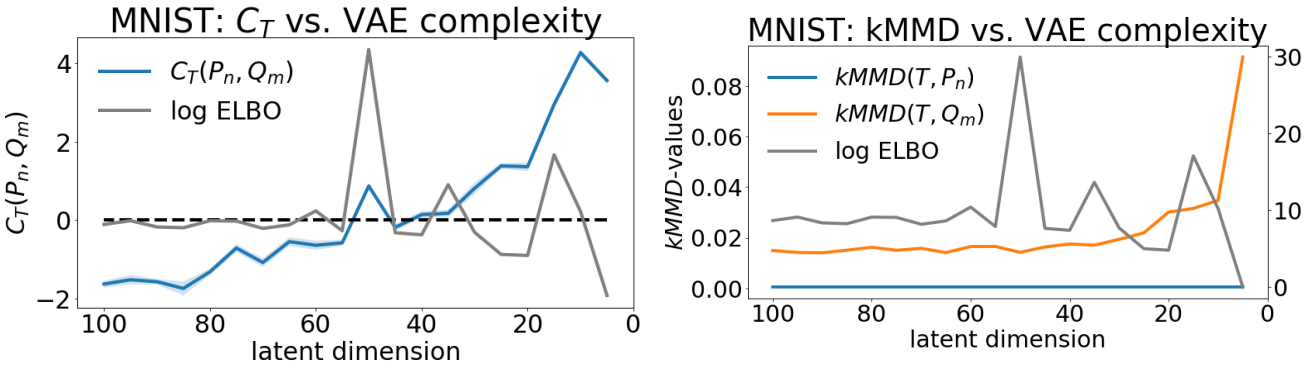

(a) $C_T(P_n, Q_m)$ **(b)** kernel MMD

Figure 11: Comparison of the $C_T(P_n, Q_m)$ test presented in this paper alongside the three sample kMMD test.

More recent works such as Esteban et al. (2017) have repurposed this test for measuring generative model overfitting. Intuitively, if the model is overfitting its training set, the empirical kMMD between training and generated data may be smaller than that between training and test sets. This may be triggered by the data-copying variety of overfitting.

This test provides an interesting benchmark to consider in addition to those in the main body. **Figure 11** demonstrates some preliminary experimental results repeating the MNIST VAE experiment **Figure 4a**. To implement the kMMD, we used code posted by Bounliphone et al. (2016) https://github.com/eugenium/MMD, and ran the three sample RBF-kMMD test on twenty MNIST VAEs with decreasing complexity (latent dimension). **Figure 11b** attached plots the kMMD distance to training set for both the generated (orange) and test samples (blue). We observe that this test does not appear sensitive to over-parametrized VAEs ($d > 50$) in the same way our proposed test (Figure 1a attached) is. It is sensitive to underfitting ($d << 50$), however. The p-values of that work's corresponding hypothesis test (figure not shown) similarly did not respond to data-copying.

We suspect that this insensitivity to data-copying is due to the fact that – for a large number of samples m, n – the kMMDs between T and P_n, and between T and Q_m are both likely to be near zero when Q data-copies. Consider the case of extreme data-copying, when Q_m is simply a bootstrap sample from the training set T. The kMMD estimate will be

$$\widehat{\mathrm{MMD}}^2(T, Q_m) = \sum_{x,x' \in T} k(x, x') - 2 \sum_{\substack{x \in T \\ y \in Q_m}} k(x, y) + \sum_{y,y' \in Q_m} k(y, y')$$

Informally speaking, the second and third summations of this expression almost behave identically on average to the first since Q_m is a bootstrap sample. They only behave differently for summation terms that are collisions: $k(x, y), x = y$ in the second summation, and $k(y, y'), y = y'$ in the third summation. The fraction of these collision summation terms decreases rapidly with m, n. Consequently, the kMMD between the training set and this bootstrap sample is very near zero. It is clear to see that the same goes for the kMMD between the training and test sample, since they are independent samples from the same distribution.

The experiment in **Figure 11b** does not test for extreme data-copying since the model is a VAE, not KDE. Consequently, there still is an appreciable gap between the test and generated kMMD to the training set. Regardless, this kMMD is not sensitive enough to differentiate between the well-fit model of dimension ≈ 50 and the overfit models of dimension ≈ 100.

7 Likelihood Generalization Gap Tests

Here, we repeat the experiments of **Figures 3** and **4**, this time juxtaposing with the generalization gap: the difference between the log likelihood of the training set and the test set. Naturally, a model heavily overfit on the training set will assign a very high likelihood to the training set as compared with the test set. These comparisons can only be made when the likelihood is tractable, however. As such, we only provide true generalization gap tests for the 'moons' and MNIST Gaussian-KDE experiments. For the MNIST VAE experiments, we treat the ELBO as a likelihood estimate, and plot the difference between the test and training set ELBO as model complexity ranges from high to low. We cannot create such experiments for the GAN experiments.

Figure 12 depicts this comparison between the top row (generalization gap) and bottom row (C_T statistic). The likelihood gap behaves similarly in both the 'moons' and MNIST KDEs, **Figures 12a** and **12b**. Here, the likelihood generalization gap successfully identifies data-

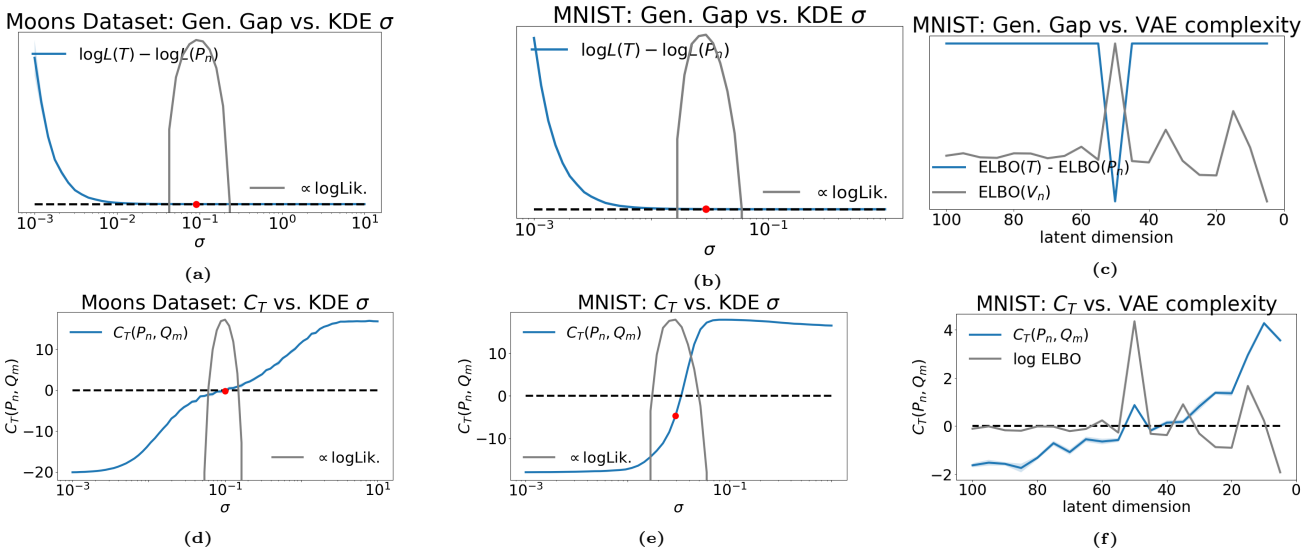

Figure 12: Comparison between the C_T test statistic (bottom row) and likelihood generalization gap (top row) for two data domains, and two model types: moons dataset KDE (left), MNIST dataset KDE (middle), MNIST dataset VAE (right).

copying when $\sigma << \sigma_{\text{MLE}}$. That said, it does not identify underfitting: when $\sigma >> \sigma_{\text{MLE}}$, the statistic reports approximately the same value it does at σ_{MLE}. This makes sense, since a high-bias underfit model Q should assign similar likelihoods to different samples from the same distribution; in this case the training sample T and test sample P_n.

Meanwhile, the ELBO generalization gap depicted in **Figure 12c** does not detect over- *or* underfitting. For values above and below the optimal model size (latent dimension ≈ 50), the ELBO gap remains approximately the same. This may be because the ELBO is not that actual likelihood but a lower bound thereof, and is an inaccurate surrogate.

We believe these experiments further indicate the utility of the C_T test statistic for evaluating generative models. It's ability to capture overfitting parallels that of the canonical likelihood generalization gap test, and even exceeds it when checking for underfitting.